Regular Article

PHYSICAL CHEMISTRY RESEARCH
Published by the
Iranian Chemical Society
www.physchemres.org
info@physchemres.org

Phys. Chem. Res., Vol. 9, No. 3, 539-552, September 2021
DOI: 10.22036/pcr.2021.276552.1902

Photocatalytic Degradation of Ethylbenzene in Aqueous Solutions by $ZnFe_2O_4$ Nanoparticles Supported on the Copper Slag: Optimization, Kinetics and Thermodynamics Studies

H. Malekhosseini[a] and K. Mahanpoor[b,*]

[a]*Department of Chemistry, North Tehran Branch, Islamic Azad University, Tehran, Iran*
[b]*Department of Chemistry, Arak Branch, Islamic Azad University, Arak, Iran*

(Received 2 April 2020, Accepted 14 May 2021)

$ZnFe_2O_4$/copper slag (CS), an environmentally friendly and cost-effective catalyst, was produced by co-precipitation methods and a thermal process. The synthesized catalyst was characterized by XRD, SEM, EDX and BET surface area analyses. The X-rays diffraction pattern confirmed that the crystal structure of $ZnFe_2O_4$ after stabilization on CS zeolite has not changed. The SEM images showed that despite their varying sizes, the particles all have the same shape. Photocatalytic activity of the catalyst was tested for the degradation of ethylbenzene (EB) in water by UV + H_2O_2 method in a reverse-flow packed bed photo reactor. The process optimization and modeling were performed using the full factorial method. The best conditions were found to be 30 ppm the initial EB concentration, pH = 9, and 15 ppm the initial H_2O_2 concentration. Under ideal process conditions, the removal efficiency of EB was greater than 99.5%. The validity of the Langmuir-Hinshelwood kinetics model was confirmed using EB photocatalytic degradation experimental results. The values of $\Delta H^{\#}$ and $\Delta S^{\#}$ for the photocatalytic degradation of EB by $ZnFe_2O_4$/CS catalyst in the UV + H_2O_2 process were calculated based on the transition state theory and gave 1.67 kJ mol^{-1} and -263.057 J K^{-1} mol^{-1}, respectively.

Keywords: Photocatalytic process, Mathematical modeling, Experimental design, UV + H_2O_2

INTRODUCTION

Water pollution is a major cause of concern in most of the developing countries. The chemical industries produce a large amount of waste water containing toxic pollutants [1,2].

Ethylbenzene (EB) is an important material in the petrochemical industry as a medium for the production of styrene. Styrene is the main precursor for the production of polystyrene (a general plastic material). This substance can penetrate into the effluents of these industries and cause effluent pollution. Several methods of industrial wastewater degradation have been performed worldwide [2]. Photocatalytic processes are a promising method for the degradation of various hazardous chemicals found in effluents.

The importance of this method is that it can eliminate various complex organic chemicals in the effluent, which cannot be eliminated by other methods. These processes frequently include the addition of an oxidizing agent, such as hydrogen peroxide, in the presence of a catalyst under UV light irradiation. In this condition, highly reactive radicals such as hydroxyl radicals are formed and mineralize organic contaminants, converting them to carbon dioxide, water and to inorganic anions. The advantages of photocatalytic degradation over conventional degradation treatment techniques include lower cost, mild operating conditions and wide range of organic pollutants [1,3]. For the specific contaminant studied in this research work, aqueous solution of EB, there are some reports of photocatalytic degradation with different catalysts and various conditions. Titanium dioxide, TiO_2/UV/O_3 and transition metal-doped titanium dioxide immobilized on

*Corresponding author. E-mail: k-mahanpoor@iau-arak.ac.ir

fiberglass cloth are examples of catalyst (or condition) used for the photocatalytic removal of EB in these research studies [4-6].

Recently, $ZnFe_2O_4$ as a catalyst for photocatalytic degradation has attracted the attention of researchers to remove hazardous contaminants in water [7]. The most important problems in photocatalytic processes, including the accumulation of the catalyst and its small specific surface area, can be solved by fixing the catalyst on a suitable base. Copper slag is a cheap and very stable compound with appropriate mechanical and thermal properties, so it is suitable for use as a catalyst base [8]. Copper slag is a combination of silicates and metal oxides that are separated from copper ore impurities when copper is removed from a furnace. When copper is melted, the impurity floats on the molten metal to form angled granules. This material is either disposed of as a waste or used as an abrasive to clean metal surfaces and disposed of as a waste after use [8]. The use of this substance as a base catalyst is one of the innovations of this research. The use of reverse flow packed bed reactor and determination of kinetic and thermodynamic parameters in this reactor can also be considered innovations of this research.

The experimental design is one of the best tools for studying the effect of process operational parameters separately as well as their interaction effects simultaneously. Numerous studies have been carried out to investigate the application of design of experiments in different processes [9].

In this study, the experimental design was performed by the full factorial method with respect to variables including pH, the initial concentration of H_2O_2 and the concentration of EB in the solution [10]. The effect of each variable separately and their interaction effects were studied simultaneously through analysis of variance (ANOVA). The optimal conditions were determined and the appropriate experimental mathematical model for the UV + H_2O_2 process by $ZnFe_2O_4$/CS photocatalyst.

MATERIALS AND METHODS

Materials

The CS was purchased from the Masbareh Sazan Jonoob Company (Iran) and other materials used in this research were purchased from the Merck Company (Germany).

Preparation and Characterization of $ZnFe_2O_4$/CS

A method similar to the previous study was used to prepare the catalyst [11]. According to this method, 100 ml of 0.5 M solution of zinc nitrate prepared from $Zn(NO_3)_2.6H_2O$ was added to 100 ml of 1 M iron nitrate solution (prepared from $Fe(NO_3)_3.9H_2O$). Then, 100 ml of 1 M urea solution was added to this solution and heated in a boiling water bath for 8 h (under reflux conditions). The precipitate after separation from the solution was dried in an oven at 110 °C and ground in a porcelain mortar. This powder was mixed with ethanol and added to the CS. Having dried at room temperature, $ZnFe_2O_4$ was stabilized on the CS by a calcination method. The powder was placed in an oven at 550 °C for 6 h. The product was $ZnFe_2O_4$ catalyst that was stabilized on CS. After stabilization of the catalyst on the CS, the mass percent of stabilized $ZnFe_2O_4$ was 8.37%.

The X-Ray diffraction (XRD) analysis of the samples was done by a DX27-mini diffractometer. The shape, size, surface morphology and the atomic percentage of samples were determined using the SEM images and EDX analysis obtained by a Philips XL-30 SEM device. The BET surface area of materials was determined by the N_2 adsorption-desorption method of 77 K, measured by BELSORP-mini II instruments. The samples were degassed under a vacuum at 473 K for 12 h before the BET measurement.

Experimental Setup

The experimental procedure was done by circulating packed bed reactor (CPBR). A schematic plan of the device is shown in Fig. 1. CPBR with one UV lamp (15 W Philips) and a volume of 1 l that was filled with 70 g of catalyst $ZnFe_2O_4$/CS was used for photocatalytic degradation of EB in aqueous solution. To control the temperature at 25 °C in all experiments, a photo reactor with a water flow jacket connected to a thermo-bath (model ALB64, Korean company FINEPCR) was used. Metrohm pH meter model 827 was used for pH measurement. H_2SO_4 and NaOH diluted solutions were used to adjust the pH of solutions and different volume levels of hydrogen peroxide were added to the EB solution. The solutions are transferred to the feed

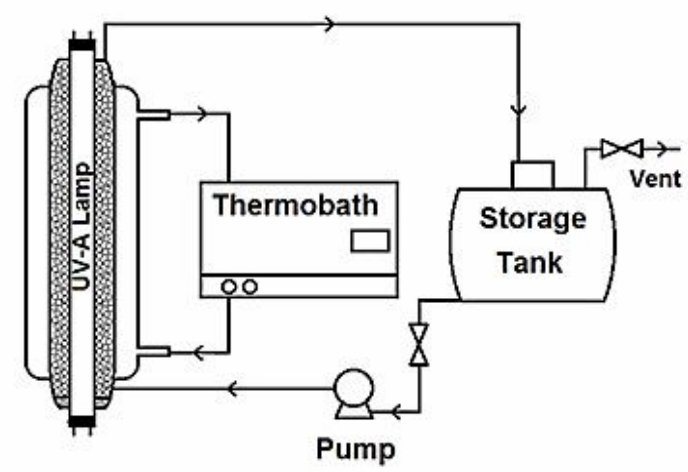

Fig. 1. Schematic of the experimental process.

tank and sent to the reactor by a water pump. After half an hour of rotating the solution inside the reactor, the UV lamp was turned on. Samples were taken every 10 min and their COD was measured by a standard method (5220). The percentage removal was calculated by using the following equation:

$$x\% = \frac{COD_0 - COD}{COD_0} \times 100 \quad (1)$$

where x is removal efficiency (%), COD_0 is the initial chemical oxygen demand value of EB solution and COD is the chemical oxygen demand value of solution after photo-irradiation.

Experimental Design

The full factorial experimental design was used with 11 experiments according to Table 1. Statistical data were analyzed based on the analysis of variance (ANOVA). The independent variables considered to evaluate the photocatalytic oxidation process were pH, EB initial concentration, and H_2O_2 initial concentration at three levels. The level values of each variable were selected using initial experiments and previous research. The variables and their levels, as well as the necessary experiments, are given in Table 1. The statistical software Minitab 17 was design and analyze the experiments.

RESULTS AND DISCUSSION

Catalyst Identification

The XRD, SEM and BET techniques were used to identify the catalyst. The powder X-ray diffraction (XRD) pattern of the obtained $ZnFe_2O_4$ provides additional crystallinity and phase detail. The observed peak positions (as shown in Fig. 2) are consistent with those stated in the literature for $ZnFe_2O_4$ [12]. The major crystalline phases present in CS were Fayalite ($2FeO.SiO_2$) specified peaks at the 2θ = 52, Magnetite (Fe_3O_4), Hedenbergite Ca (Fe, Mg) $(SiO_3)_2$, Hematite and Maghemite specified peaks in the range of 2θ = 28-31, which are consistent with previous research [13]. Also, no change in the diffraction angle of $ZnFe_2O_4$ peaks after stabilization on CS is observed, so the crystal structure of $ZnFe_2O_4$ after stabilization on CS has not changed. Furthermore, the Debye-Scherrer formula is used to measure the mean sizes of the synthesized nanoparticles from the peak broadening in the XRD pattern. $ZnFe_2O_4$ has an average size of 65 nanometers.

Scanning electron microscopy was used to determine the surface morphology and estimated particle size of $ZnFe_2O_4$. The results (Fig. 3) show that the particles have a smooth, homogeneous surface and are very similar. Although the size of the particles varies, they all have the same shape. All of the surfaces of the CS have been coated with $ZnFe_2O_4$ nanoparticles, as shown in Fig. 3. The product's EDX

Table 1. Experimental Conditions and EB Degradation Percentages for Photocatalytic Process

Run	pH	Initial concentration of EB (ppm)	H_2O_2 Initial concentration (ppm)	Experimental results for removal efficiency (%x)	Fit
1	5	30	5	44.12	43.8325
2	9	30	5	68.45	68.4050
3	5	70	5	33.15	33.4375
4	9	70	5	47.50	47.5450
5	5	30	15	65.32	65.6075
6	9	30	15	99.55	99.5950
7	5	70	15	55.50	55.2125
8	9	70	15	78.78	78.7350
9	7	50	10	61.54	61.5567
10	7	50	10	60.98	61.5567
11	7	50	10	62.15	61.5567

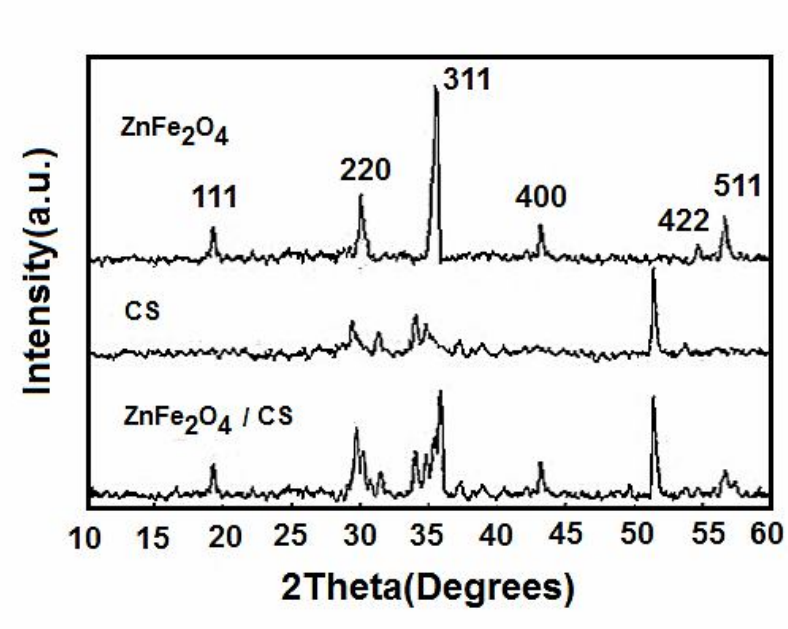

Fig. 2. The XRD patterns of photocatalyst $ZnFe_2O_4$, CS and $ZnFe_2O_4$/CS.

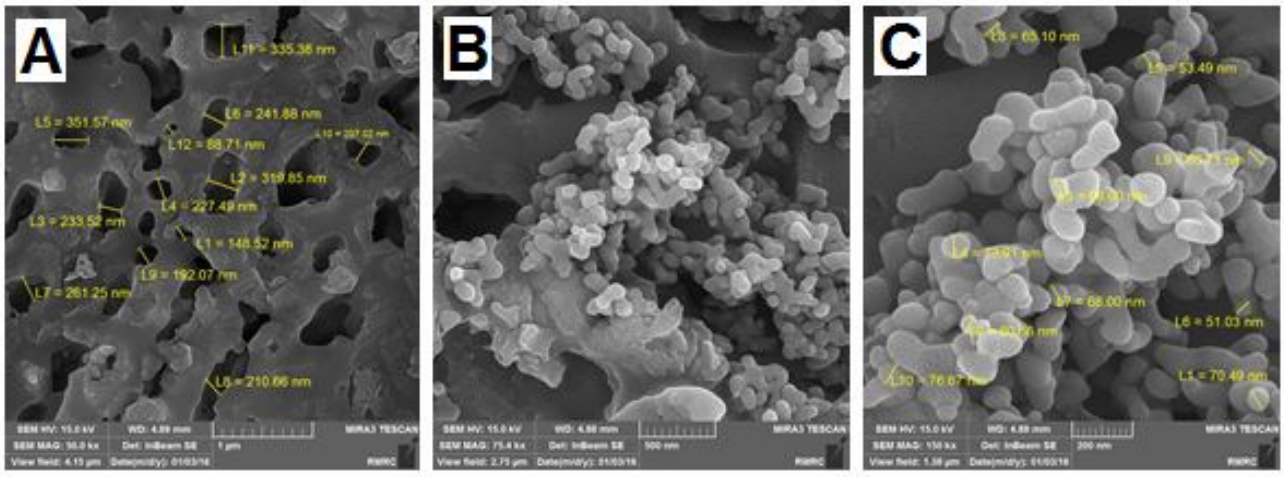

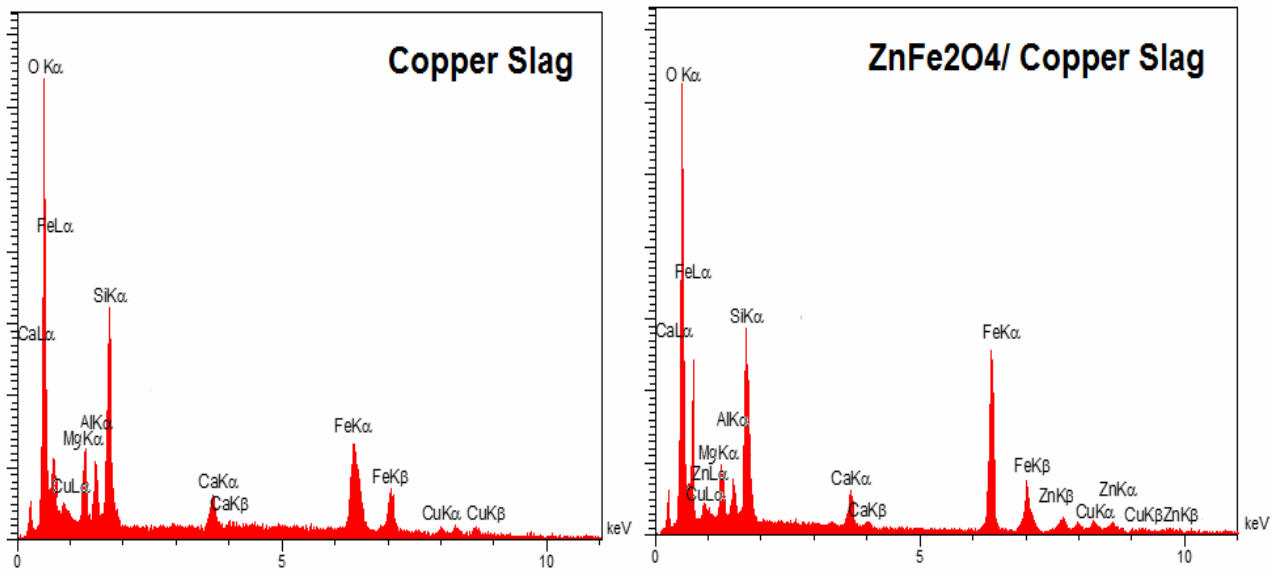

Materials	Unit	O	Mg	Al	Si	Ca	Fe	Cu	Zn
CS	Weight%	36.12	2.11	1.08	16.17	4.64	38.23	0.56	-
	Atomic%	59.27	2.31	1.05	16.17	3.05	17.92	2.31	-
$ZnFe_2O_4$/CS	Weight%	31.72	1.82	0.95	15.14	4.11	39.32	0.47	6.47
	Atomic%	56.56	2.16	1.01	15.42	2.93	20.03	0.21	1.68

Fig. 3. SEM images and their EDX analysis of CS (A) and $ZnFe_2O_4$/CS (B, C).

analysis revealed that the material produced on the surface could contain $ZnFe_2O_4$ nanoparticles (due to changes in the atomic percent of copper slug and $ZnFe_2O_4$/CS).

Pore structure analysis of porous materials is performed using nitrogen adsorption-desorption isotherms at low temperatures (77 K). The surface area of samples is determined using the Brunauer-Emmett-Teller (BET) process. The adsorption-desorption isotherms and BET surface area for the CS and $ZnFe_2O_4$/CS are shown in Fig. 4. According to previous research [14], for CS and $ZnFe_2O_4$/CS, the presented type IV isotherm and type H2 hysteresis loops are typical of mesoporous materials with bottleneck (cylindrical pore geometry) pores and spherical particles arranged in a fairly uniform manner. The BET surfaces' area of CS and $ZnFe_2O_4$/CS were determined 3.21 and 16.25 (m^2 g^{-1}), respectively. Supporting nanoparticle $ZnFe_2O_4$ on the CS appears to have an increased surface area of BET catalyst.

Optical Property and Photocatalytic Mechanism

The optical properties of the $ZnFe_2O_4$ were measured using UV-Vis diffuse reflectance spectroscopy (DRS) (Varian Cary 100 UV-Vis Spectrophotometer with DRA-CA-30IDiffuse Reflectance Accessory). A band gap is the distance between the valence band of electrons and the conduction band. The band gap is the minimum amount of energy needed to excite an electron to a location in the conduction band. The band gap energy can be calculated by the formula $E_g = 1240/\lambda_{onset}$, where λ_{onset} is the absorption onset wavelength. As shown in Fig. 5, $ZnFe_2O_4$ mainly absorbs light with a wavelength of 523 nm, and the band gap energy of ZnFe2O4 was calculated to be 2.37 eV.

The mechanism of photocatalytic reactions by $ZnFe_2O_4$ supported on the CS is similar to other semiconductors. This is because when $ZnFe_2O_4$ is illuminated by light with a wavelength equal to or greater than the band gap (2.37 eV), the electrons are upgraded from the capacitance band to the semiconductor oxide conduction band, forming the electron-hole pairs as follows [15-18]:

$$ZnFe_2O_4/CS + h\nu \rightarrow ZnFe_2O_4/CS\ (e^-_{CB} + h^+_{VB}) \quad (1)$$

The valence band (h^+_{VB}) potential is positive enough to generate hydroxyl radicals as follows:

$$h^+_{VB} + H_2O_{(ads)} \rightarrow H^+ + {}^{\bullet}OH_{(ads)} \quad (2)$$

The conduction band (e^-_{CB}) potential is negative enough to reduce molecular oxygen and produce superoxide radical ions ($^{\bullet}O^-_{2(ads)}$).

$$e^-_{CB} + O_{2(ads)} \rightarrow {}^{\bullet}O^-_{2(ads)} \quad (3)$$

Superoxide radical ions can react with water to form hydroxyl radicals.

Hydrogen peroxide absorbs a photo-electron and produces the hydroxide radical in the next reaction (reaction 4) [18].

$$H_2O_2 + e^-_{CB} \rightarrow {}^{\bullet}OH_{(ads)} + OH^- \quad (4)$$

Also, under ultraviolet light, hydrogen peroxide creates hydroxide radicals by the following reaction:

$$H_2O_2 + h\nu \rightarrow 2{}^{\bullet}OH \quad (5)$$

Water can react with superoxide radical ions to form hydroxyl radicals. Strong oxidizing agents such as hydroxyl radicals and superoxide radical ions target EB molecules on or near the surface of $ZnFe_2O_4$/CS as follows:

$$({}^{\bullet}OH_{(ads)} \text{ or } {}^{\bullet}O^-_{2(ads)}) + EB \rightarrow \text{degradation of the EB} \quad (6)$$

Factorial Design Modeling of the Experiments

To optimize the photocatalytic processes, successful variables such as pH, EB initial concentration (ppm), and H_2O_2 initial concentration should be evaluated. Single factor analysis would be a long, incomplete, and complex method if these factors were not independent. A detailed analysis is provided by modeling using the factorial design process. This approach has the benefit of saving time and having fewer trials to refine the procedure. This approach can also be used to define how variables communicate. The complete factorial design approach was used to investigate the photocatalytic degradation of EB in aqueous solutions, and the results are shown in Table 1. A regression analysis

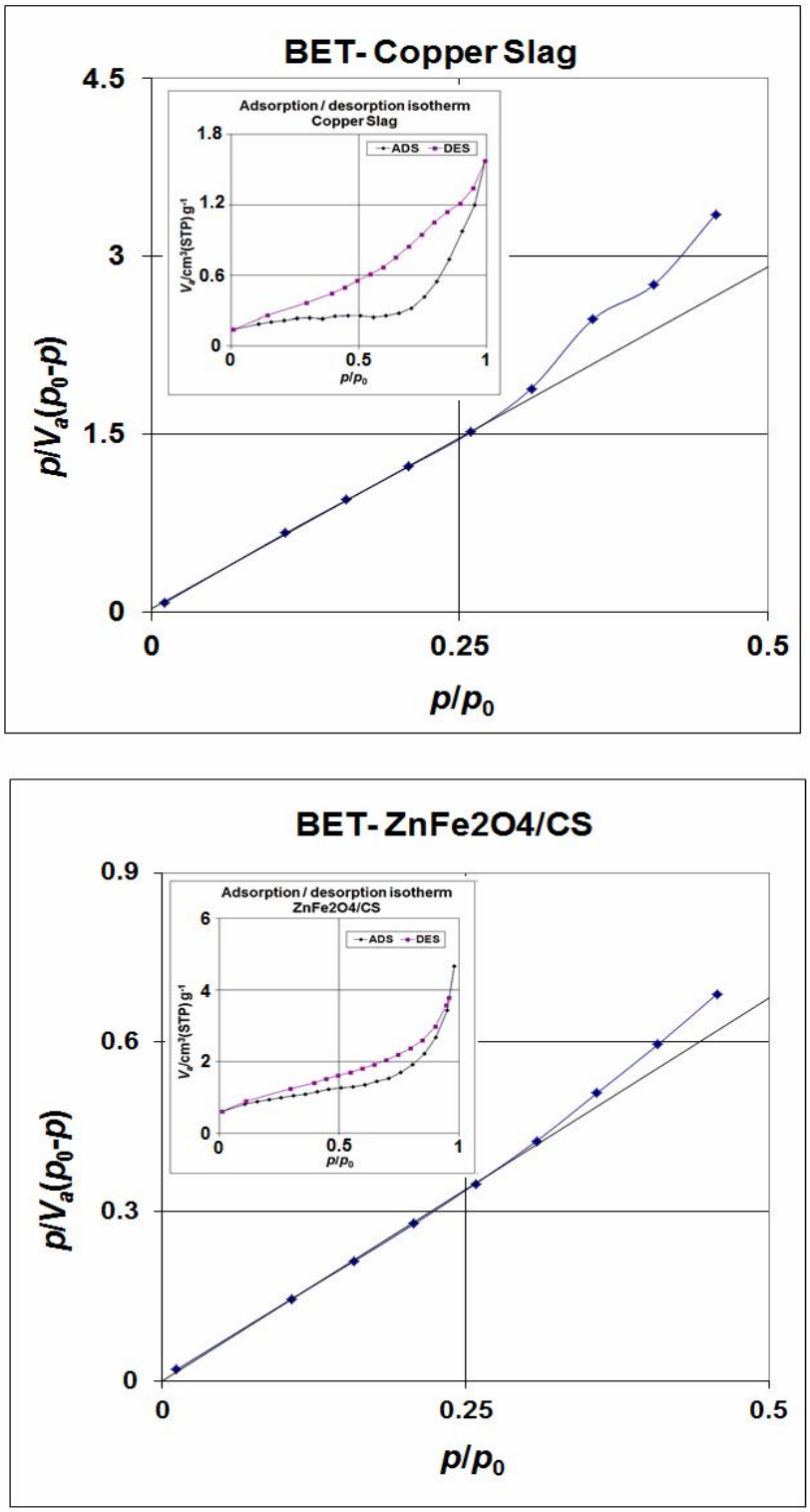

Fig. 4. Adsorption-desorption isotherms and BET surface area for the CS and $ZnFe_2O_4$/CS.

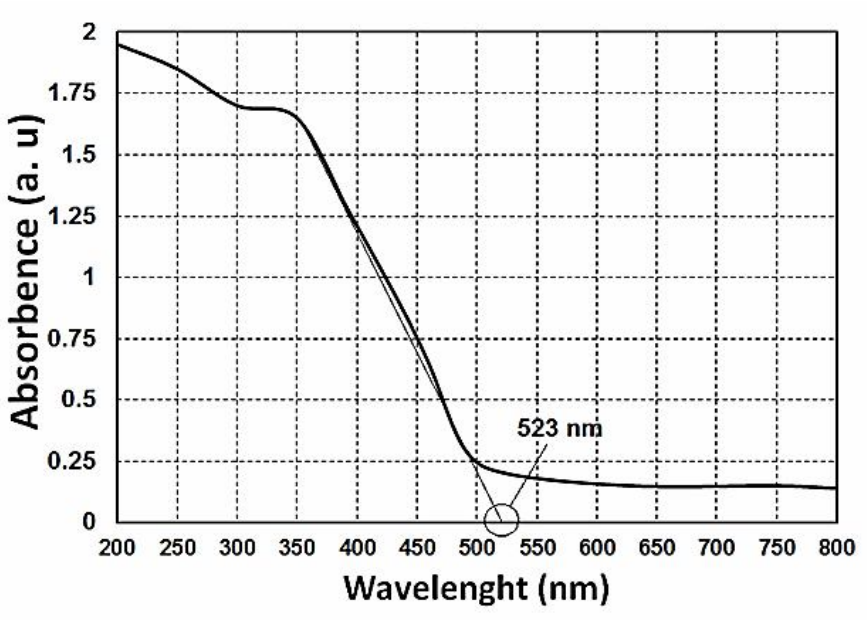

Fig. 5. Diffuse reflectance spectra of $ZnFe_2O_4$.

Table 2. The Values of P and F Parameters in Term of Responses

Term	Coefficients	T-value	F-value	P-value
Constant	61.546	344.12	3073.49	0.0000
pH	12.024	67.23	5648.23	0.0001
EB	-7.814	-43.69	2385.35	0.0000
H_2O_2	13.241	74.04	6850.00	0.0000
pH × EB	-2.616	-14.63	267.42	0.0003
pH × H_2O_2	2.354	13.16	216.45	0.0002

Table 3. Results of ANOVA for Photocatalytic Degradation of EB

Response	Source	Degree of freedom	Sum of square	Mean square	F
EB degradation	Regression	6	3146.73	524.45	2049.47
	Residual error	4	1.02	0.026	
	Total	10	3147.75		
$R^2_{pre} = 99.78$, $R^2_{adj} = 99.92$					

approach is used to analyze the statistical model of sample data. Equation (2) represents the mathematical model:

$$x\% = 6.10 + 6.928A + 0.0672B + 1.001C - 0.06541A \times B + 0.2354A \times C \quad (2)$$

where A, B and C are pH, initial concentration of EB and H_2O_2 initial concentration, respectively.

The ANOVA test is one of the most effective methods for determining the importance of experiment results. The study of variance takes the method of comparing the means of two samples and applies it to several samples.

The R^2 coefficient and the Fisher test (F-test) were used to assess the polynomial model's accuracy and statistical significance. The predicted effects and x percent coefficients are mentioned in Table 1. The coefficient of determination was calculated as the square of the correlation coefficient for each answer (R^2). R^2 may be used to assess the model's accuracy and variability. R^2 always has a value between 0 and 1. The closer R^2 is to 1, the more accurately the model predicts the responses (x%). The R^2 value obtained in this paper was 0.999. The R-squared coefficient determination values (0.9983) are close to the modified "R-squared" coefficient (0.9996), indicating that this model is well-predictable. The coefficients of pH, initial concentration of EB, and initial concentration of H_2O_2 were calculated to be 12.024, -7.814 and 13.241, respectively, based on Table 2 and the significant effects of the variables in the reaction. As a result, the impact of these variables can be determined as follows:

Initial concentration of EB < pH solution < soluble H_2O_2 concentration

It should be noted, however, that when other variables are present, the initial concentration of EB has a negative impact on the response (-7.814). It implies that as the initial concentration of EB rises, the percentage decreases by %x, and vice versa. Table 2 shows the interaction effects of variables in the same way. These findings, as well as the interaction of variables, lead to the conclusion that simultaneous interactions of the three variables, as well as the interaction of initial EB concentration with H_2O_2 concentration, have no important effect (P-value > 0.05). The interaction of initial H_2O_2 concentration with pH has a positive effect on the value of x percent (2.354). The ANOVA results are shown in Table 3. Decreasing the value of parameter P and increasing the value of parameter F have incremental effects on the responses.

Residues are usually recognized by the fitted model as an unjustifiable improvement, and they are assumed to have a normal distribution. The analysis of plots with normal likelihood is an effective method for determining the normality of the residues. The normal distribution in the natural probability diagram (Fig. 6a) depicts the expected response values *versus* the residual values. Figure 6b shows a graph of the residual versus the fitted value (predicted response) that shows random behavior with no bias towards residuals for the experimental value. The normal distribution of residual values is verified by the histogram diagram in Fig. 6c. Figure 6d indicates that the residual graphs display random scatter versus data order, indicating that the t statistic is adequate.

By ignoring interactions, it is possible to conclude that the initial concentration of EB has the greatest impact on the degradation process. The degradation percentage increased dramatically as the amount of $ZnFe_2O_4$/CS increased. The development of hydroxide radicals increases as the amount of $ZnFe_2O_4$/CS increases. The amount of catalyst used after EB concentration has a major impact on photocatalytic degradation processes. As a result, as the amount of catalyst increases, so does photocatalytic degradation. The next stages of control on the photocatalytic degradation of EB are H_2O_2 concentration and pH. H_2O_2 is an effective advanced oxidation agent that has a significant impact on photocatalytic reaction rates. The generation of hydroxide radicals by photolysis of hydrogen peroxide as a powerful oxidant improves the efficiency of decomposition processes (Eq. (4)). Moving the pH from 5 to 9 affects the percentage of deterioration. The propensity of OH^- ions at the $ZnFe_2O_4$/CS level to form hydroxide radicals can explain the high degradation efficiency of EB in alkaline conditions [18].

Kinetic of Photocatalytic Degradation of EB

In an ideal condition, $\ln(A_0/A)$ was plotted against reaction time for EB photocatalytic decomposition (Fig. 7). The reaction kinetic is pseudo-first-order with a rate

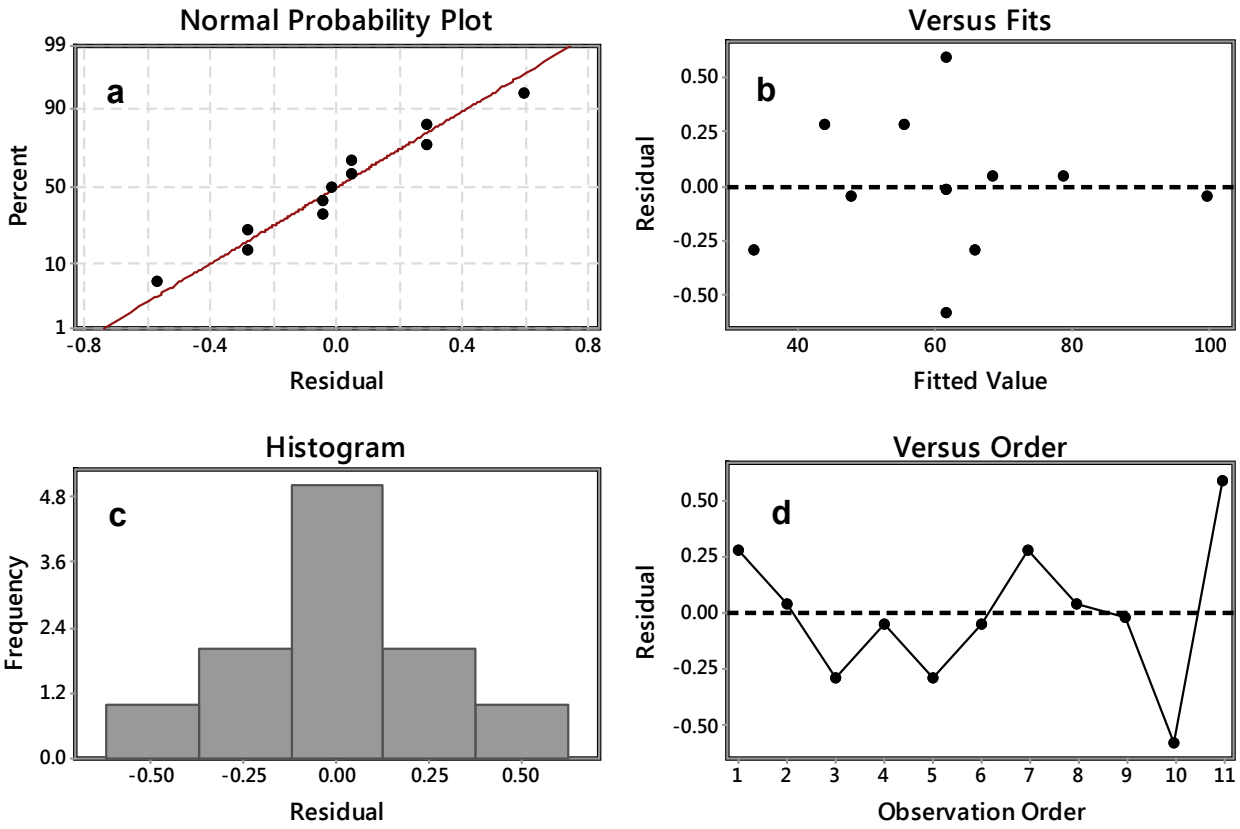

Fig. 6. (a) Normal probability plot, (b) residual value compared to fitted values, (c) histogram of the effect of standardized factors and (d) residual values compared to observation order.

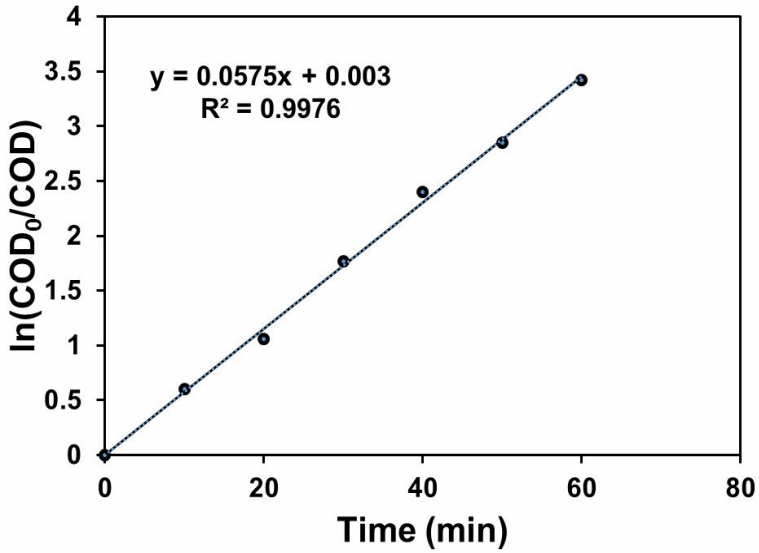

Fig. 7. Kinetic plot of $\ln(A_0/A)$ *versus* irradiation time for EB photocatalytic degradation. Initial concentration of EB = 30 ppm, initial concentration of H_2O_2 = 15 ppm, and pH = 9.

coefficient of k = 0.0575 min^{-1}, as shown by the graph's linearity.

The Langmuir-Hinshelwood kinetic model is often used to describe the kinetics of heterogeneous photocatalytic processes (Eq. (3)) [19],

$$r = \frac{dC}{dt} = \frac{k_r K_e C}{1 + K_e C} \quad (3)$$

where r is the reaction rate, C is the concentration of EB, k_r and K_e are the apparent reaction rate constant and the apparent equilibrium of adsorption constant, respectively. By replacing r with the initial reaction rate r_0 and C_0 with the initial concentration of EB in the raw effluents, Eq. (4) can be written in the following linearized form:

$$\frac{1}{r_0} = \frac{1}{k_r K_e C_0} + \frac{1}{k_r} \quad (4)$$

In order to determine the values of k_r and K_e using the initial rate method, a series of experiments were carried out with varying initial concentration of EB. Figure 8 shows the plot of $(1/r_0)$ against $(1/C_0)$ with very high correlation coefficient (R^2 = 0.9939). The calculated values of k_r and K_e were 18.8 mg l^{-1} min^{-1} and 3.07 × 10^{-3} mg l^{-1}, respectively. The EB adsorption is the controlling step of the photocatalytic process because the value of k_r is substantially higher than that of K_e.

To evaluate the effect of temperature on the reaction rate, experiments were performed in the temperature range of 298-313 K. The results showed that with increasing temperature, the reaction was somewhat accelerated.

The Arrhenius equation was used to calculate the reaction activation energy (E_a) and frequency coefficient (A) [20]:

$$\ln k_{app} = -\frac{E_a}{R(\frac{1}{T})} + \ln A \quad (5)$$

where R and T are the universal gas constant (8.314 J K^{-1} mol^{-1}) and absolute temperature (K), respectively. E_a and A were obtained from the slope and intercept of the $\ln k_{app}$ *vs.* 1/T plot (Fig. 9), which respectively gave 4.205 kJ mol^{-1} and 0.313 min^{-1}.

Calculation of Activation Parameters

The activation parameters in the photocatalytic degradation of EB by $ZnFe_2O_4$/CS were studied using the Eyring's transition state theory (TST) [21]. According to this theory, the reaction rate of $(A + B \underset{k_{-1}}{\overset{k_1}{\rightleftarrows}} AB^{\mp} \rightarrow \Pr oducts)$ can be described as follows:

$$\ln\left(\frac{k_{app}}{T}\right) = -\frac{\Delta H^{\mp}}{R}\frac{1}{T} + \frac{\Delta S^{\mp}}{R} + \ln\left(\frac{k_B}{h}\right) \quad (6)$$

where k_B, h, k_{app}, $\Delta H^{\#}$ and $\Delta S^{\#}$ are respectively the constants of Boltzmann (1.38 × 10^{-23} J K^{-1}), Plank (6.62 × 10^{-34} J s^{-1}), appearance rate constant, activation enthalpy and activation entropy.

The values of $\Delta H^{\#}$ and $\Delta S^{\#}$ for the photocatalytic degradation of EB by $ZnFe_2O_4$/CS were calculated from the slope and intercept of the $\ln(k_{app}/T)$ *vs.* 1/T plot (Fig. 10), which respectively gave 1.67 kJ mol^{-1} and -263.057 J K^{-1} mol^{-1} values. This means that, the photocatalysis process is endothermic ($\Delta H^{\#} > 0$) with increasing regularity at the interface of EB molecules/ catalyst ($\Delta S^{\#} < 0$). In addition, the calculation of $\Delta G^{\#}$ at different temperatures using the relationship of $\Delta G^{\#} = \Delta H^{\#} - T\Delta S$ disclosed that the involved process was not spontaneous.

CONCLUSIONS

The stabilization of $ZnFe_2O_4$ nanoparticles on the surface of CS has enhanced its photocatalytic activity. According to the results of statistical analysis, the accuracy of the model developed in this study is statistically significant.

Three parameters including initial EB concentration, pH and H_2O_2 concentration affected %x values in the degradation of EB by photocatalytic method with $ZnFe_2O_4$/CS as a catalyst. The interaction of variables is crucial and should be taken into account during optimizing the experiment conditions, because it has a direct impact on the value of %x. pH = 9, CEB = 30 ppm and H_2O_2 = 15 ppm are the best conditions for $ZnFe_2O_4$/CS to degrade EB, with a cumulative degradation of 99.59 percent. The kinetics of EB photocatalytic degradation processes adopt the

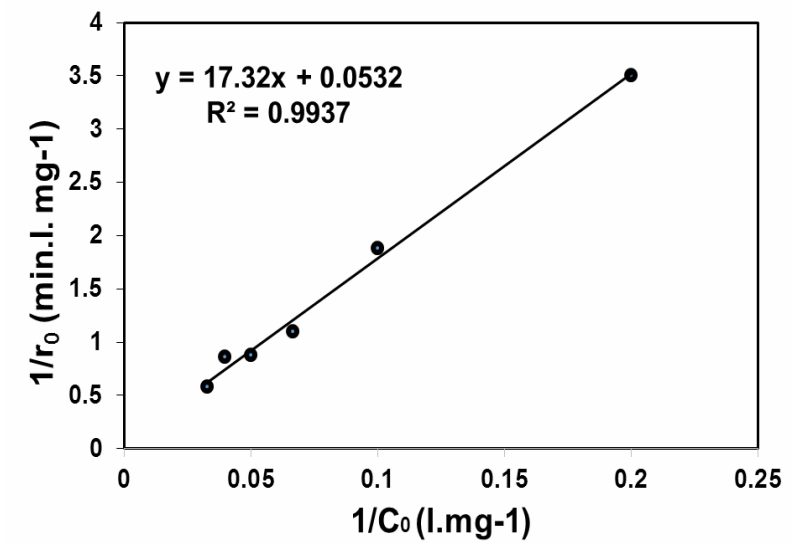

Fig. 8. Langmuir-Hinshelwood kinetics plot for photocatalytic removal of EB using $ZnFe_2O_4$/CS. Initial concentration of EB = 30 ppm, initial concentration of H_2O_2 = 15 ppm, and pH = 9.

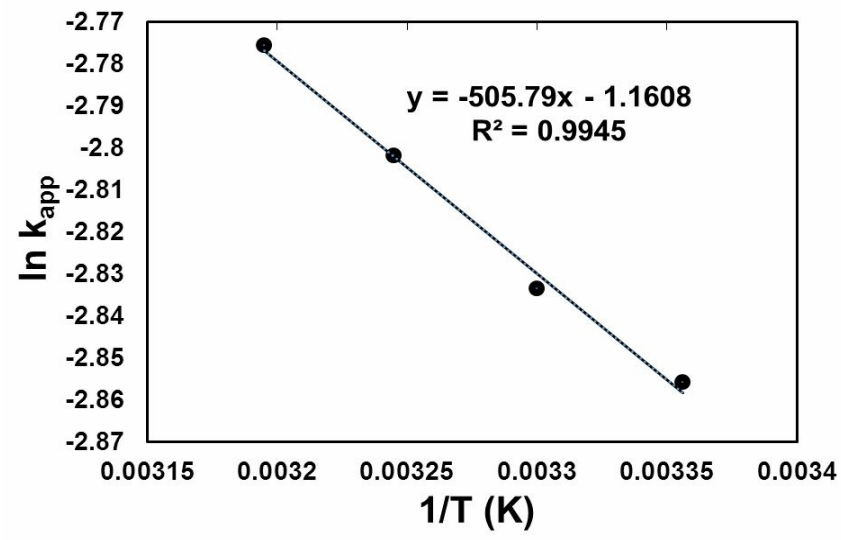

Fig. 9. Arrhenius plot for photocatalytic removal of EB using $ZnFe_2O_4$/CS. Initial concentration of EB = 30 ppm, initial concentration of H_2O_2 = 15 ppm, and pH = 9.

Langmuir-Hinshelwood kinetic model, according to the findings of this report. Using Eyring's transition state theory, the thermodynamics of the photoctalytic degradation of EB by $ZnFe_2O_4$/CS were investigated. The findings indicate that this phase is endothermic ($\Delta H^{\#} > 0$) and has an increased regularity ($\Delta S^{\#} < 0$).

ACKNOWLEDGMENTS

The authors wish to thank the Islamic Azad University

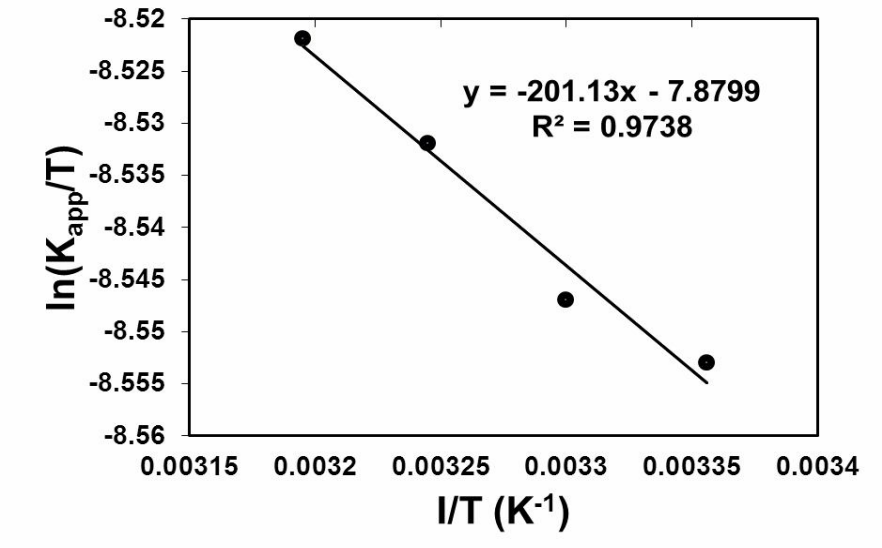

Fig. 10. Eyring plot for photocatalytic removal of EB using $ZnFe_2O_4$/CS. Initial concentration of EB = 30 ppm, initial concentration of H_2O_2 = 15 ppm, and pH = 9.

of Arak and North Tehran Branch.

REFERENCES

[1] Gopinath, K. P.; Madhav, N. V.; Krishnan, A.; Malolan, R.; Rangarajan, G., Present applications of titanium dioxide for the photocatalytic removal of pollutants from water: A review, *J. Environ. Manage.* **2020**, *270*, 110906, DOI: 10.1016/ j.jenvman.2020.110906.

[2] Pavithra, K. G.; Kumar, P. S.; Jaikumar, V.; Rajan, P. S., Removal of colorants from wastewater: A review on sources and treatment strategies, *J. Ind. Eng. Chem.* **2019**, *75*, 1-19, DOI: 10.1016/ j.jiec.2019.02.011.

[3] Asadzadeh-Khaneghah, S.; Habibi-Yangjeh. A., g-C_3N_4/carbon dot-based nanocomposites serve as efficacious photocatalysts for environmental purification and energy generation: A review, *J. Clean. Prod.*, **2020**, *276*, 124319-124336, DOI: 0.1016/j.jclepro.2020.124319.

[4] Ozogu A. N.; Aisien, F. A.; Udiba, U. U.; Chukwurah, N. C., Photocatalytic degradation of ethylbenzene on aqueous solutions using titanium dioxide as catalyst, *Am. J. Environ. Sci.,* **2016**, *3*, 26-32.

[5] Albuquerque, L.; Saldanha, S.; Santos, N. T. G.; Tomaz, E., Photocatalytic ethylbenzene degradation associated with ozone (TiO_2/UV/O_3) under different percentages of catalytic coating area: Evaluation of process parameters, *Sep. Sci. Technol.,* **2021**, *263*, 118344, DOI: 10.1016/ j.seppur.2021.118344.

[6] Laokiat, L.; Khemthong, P.; Grisdanurak, N.; Sreearunothai, P.; Pattanasiriwisawa, W.; Klysubun, W., Photocatalytic degradation of benzene, toluene, ethylbenzene, and xylene (BTEX) using transition metal-doped titanium dioxide immobilized on fiberglass cloth, *Korean J. Chem. Eng., **2012**, 29*, 377-383, DOI:10.1007/s11814-011-0179-1.

[7] Li, J.; Xinyong Li, X.; Yin, Z.; Wang, X.; Ma, H,; Wang, L., Synergetic effect of facet junction and specific facet activation of $ZnFe_2O_4$ nanoparticles on photocatalytic activity improvement, *Appl. Mater. Interfaces.* **2019**, *11*, 29004-29013, DOI: 10.1021/ acsami.9b11836.

[8] Huanosta-Gutiérrez, T.; Dantas, R. F.; Ramírez-Zamora, R. M.; Esplugas, S., Evaluation of copper slag to catalyze advanced oxidation processes for

the removal of phenol in water, *J. Hazard. Mater.* **2019**, *213*, 325-330, DOI: 10.1016/ j.jhazmat.2012.02.004.

[9] Gujral, G.; Kapoor, D.; Jaimini, M., An updated review on design of experiment (DOE) in pharmaceuticals, *J. Drug. Deliv. Ther.* **2018**, *8*, 147-152, DOI: 10.22270/jddt. v8i3.1713.

[10] Saghi, M.; Mahanpoor, K., Photocatalytic degradation of tetracycline aqueous solutions by nanospherical α-Fe_2O_3 supported on 12-tungstosilicic acid as catalyst: using full factorial experimental design, *Int. J. Ind. Chem.* **2017**, *8*, 297-313, DOI: 10.1007/s40090-016-0108-6.

[11] Zeynolabedin, R.; Mahanpoor, K., Preparation and characterization of nano-spherical $CoFe_2O_4$ supported on copper slag as a catalyst for photocatalytic degradation of 2-nitrophenol in water, *J. Nanostruct. Chem.* **2017**, *7*, 67-74, DOI: 10.1007/s40097-017-0216-7.

[12] Zhou, Z. H.; Xue, J. M.; Chan, H. S. O.; Wang, J., Nanocomposites of $ZnFe_2O_4$ in silica: synthesis, magnetic and optical properties, *Mater. Chem. Phys.,* **2002**, *75*, 181-185, DOI: 10.1016/S0254-0584(02)00052-4.

[13] Dimitrijević, M.; urošević, D.; Milić, S.; Sokić, M.; Marković, R., Dissolution of copper from smelting slag by leaching in chloride media, *J. Min. Metall. Sect. B-Metall.* **2017**, *53*, 407- 412, DOI: 10.2298/ JMMB170425016D.

[14] Wei, Z.; Huang, S.; Zhang, X.; Lu, C.; He, Y., Hydrothermal synthesis and photo-Fenton degradation of magnetic $MnFe_2O_4$/rGO nanocomposites, *J. Mater. Sci.: Mater. Electron., **2020**, 31*, 5176-5186, DOI: 10.1007/s10854-020-03077-4.

[15] Blourfrosh, S. K.; Mahanpoor, K., Preparation, characterization and photocatalytic performance of nano α-Fe_2O_3 supported on metal organic framework of Cd(II) for decomposition of cefalexin aqueous solutions, *Int. J. Nano Dimens.* **2021**, *12*, 113-127.

[16] Mafi, S.; Mahanpoor, K., Employing α-Fe_2O_3 /$Mn_2P_2O_7$ as a nano photocatalyst for degradation of toluene in aqueous environment, *J. Nanoanalysis.,* **2019**, *6*, 275-288, DOI: 10.22034/JNA.2019.669857.

[17] Salari, H.; Daliri, A.; Gholami, M., Graphitic carbon nitride/reduced graphene oxide/silver oxide nanostructures with enhanced photocatalytic activity in visible light. *Phys. Chem. Res.* **2018**, *6*, 729-740, DOI: 10.22036/PCR.2018.137083.1501.

[18] Ardakani, S. S.; Abghari, R.; Mirjalili, M., TiO_2@$CoFe_2O_4$ Nanofiber for the photocatalytic degradation of Direct Red 80, *Phys. Chem. Res.* **2019**, *7*, 309-325, DOI: 10.22036/ pcr.2019.158459.1567.

[19] Asenjo, N. G.; Santamaria, R.; Blanco, C.; Granda, M.; Alvarez, P.; Menendez, R., Correct use of the Langmuir-Hinshelwood equation for proving the absence of a synergy effect in the photocatalytic degradation of phenol on a suspended mixture of titania and activated carbon, *Carbon*. **2013**, *55*, 62-69, DOI: 10.1016/j.carbon.2012.12.010.

[20] Shams-Ghahfarokhi, Z.; Nezamzadeh-Ejhieh, A., As-synthesized ZSM-5 zeolite as a suitable support for increasing the photoactivity of semiconductors in a typical photodegradation process, *Mater. Sci. Semicond. Proc.* **2015**, *39*, 265-275, DOI: 10.1016/ j.mssp.2015.05.022.

[21] Carvalho-Silva, V. H.; Coutinho, N. D.; Aquilanti, V., Temperature dependence of rate processes beyond arrhenius and eyring: Activation and transitivity, *Front Chem.* **2019**, *7*, 380-391, DOI: 10.3389/ fchem.2019.00380.